The International Journal of Advanced Manufacturing Technology (2018) 96:3933–3950
https://doi.org/10.1007/s00170-018-1686-6

ORIGINAL ARTICLE

A binding scheme to minimize thinning of formed tailor welded blanks

Mahmoud S. Seyam[1] · Mostafa Shazly[2] · Alaa El-Mokadem[1] · Abdalla S. Wifi[1]

Received: 3 January 2017 / Accepted: 30 January 2018 / Published online: 15 March 2018

Abstract

Weld line movements (WLM) and thinning in draw bending and deep drawing of Tailor Welded Blanks (TWBs) constitute major defects in automotive applications. The present work aims at the development of a binding scheme that improves sheet thinning and eliminates WLM. This is achieved by using controlled blank holding segmented binders (blank holders) at the boundaries of the parent sheets of the TWB and counter pins at the weld lines. Analytical models for the 2-D draw bending and 3-D deep drawing are developed to predict the required blank-holder/counter-pin forces that insures identical elongation (deformation) on both sides of the TWB and thus eliminates the WLM. The 2-D model is validated by a series of draw-bending laboratory experiments. The experimentation of the proposed force scheme produced identical elongations on both parent sheets and consequently zero weld line movement (WLM) as targeted by the analytical model and hence the feasibility of the proposed scheme is proved in practice. Additional draw-bending/box-drawing experiments are conducted to compare the proposed scheme with separate use of either segmented blank holders, weld line clamping pins or counter punch. The results showed improved reduction in thinning and elimination of WLM when the binding forces of the process are controlled as proposed by the developed model.

Keywords Tailor welded blanks · Formability · Segmented binders · Draw-bending · Box deep drawing · Weld line movement · Finite element analysis

Nomenclatures

f	Tensile force along the deformed profile (normal to the sheet thickness)
$\mathrm{BHF_s}$	Blank holding force on the stronger side
$\mathrm{BHF_w}$	Blank holding force on the weaker side
F_{pin}	Clamping force along the weld line
μ_{p}	Friction coefficient at the weld line
μ_{s}	Friction coefficient at the stronger side
μ_{w}	Friction coefficient at the weaker side
K	Strength coefficient (in the maximum principal direction)
n	Strain hardening exponent
L_{o}	Original length (for each parent sheet s and w)
t_{o}	Original thickness (for each parent sheet s and w)
L	Current length (for each parent sheet s and w)
t	Current thickness (for each parent sheet s and w)
$\Delta L_{\mathrm{s_{tot}}}$	Total increase in the original length (the total elongation) of the stronger parent sheet
$\Delta L_{\mathrm{w_{tot}}}$	Total increase in the original length (the total elongation) of the weaker parent sheet
c	Die/punch clearance
R_{d}	Die corner radius
R_{p}	Punch corner radius
Y	Punch current vertical position
θ	Wrap Angle
M	Internal bending moment (for each parent sheet s and w)
X_{w}	Initial weld line position
σ	Maximum principal stress
ϵ	Maximum principal strain
α	Stress ratio $\frac{\sigma_2}{\sigma_1}$
β	Strain ratio $\frac{\epsilon_2}{\epsilon_1}$

✉ Mostafa Shazly
mostafa.shazly@bue.edu.eg

[1] Department of Mechanical Design and Production, Faculty of Engineering, Cairo University, Giza, Egypt

[2] Mechanical Engineering Department, Faculty of Engineering, The British University in Egypt, Al-Shorouk City, Cairo 11873, Egypt

1 Introduction

Innovative solutions to reduce vehicle's weight to improve fuel consumption are crucial to automotive industry. Currently, body panels in modern vehicles are constructed using Tailor Welded Blanks (TWBs) to achieve improved performance while minimizing total weight. A TWB consists of several flat metallic sheets with different characteristics (parent sheets) joined together prior to stamping to final shapes. The major success of the process, however, comes with detrimental reduction in formability as a result of the geometrical/material discontinuity [1]. The blank heterogeneity also causes diversity in the developed strains when uniform loads are applied, leading to accidental relocation of the parent sheets which is also known as Weld Line Movement (WLM).

Several attempts were made to enhance the formability of TWBs by eliminating the WLM. Ahmetoglu et al. [2] managed to control the weld line movement in deep drawn cups made of AKDQ TWB with a thickness ratio of 1.8/0.8 using segmented binders with different levels of blank holding force on each parent sheet. The blank holding force (BHF) at the thinner side was increased by 100% while simultaneously decreased at the thicker side by 80%. Kinsey and Cao [3] applied additional constrains to the weld line directly using clamping pins to prevent WLM and enhance formability. Similarly, Morishita et al. [4] used a counter punch instead of the pins. They experimentally proved that a half counter punch causes the same result of a full counterpunch if applied to the stronger side of the cup bottom, while causes early failure if applied to the weaker side. Other techniques including the adjustment of initial under binder-blank shape [4] and draw beads [5] were also capable of reducing the WLM. Chen et al. [6] studied the effect of using both stepped and flat binders during the box drawing of a 1.2/0.8 mm thick TWB. In the case of stepped binders, full contact with the thinner flange was achieved unlike the case with a flat binder where the gap between the binder and the flange prompted wrinkling. They also showed that the application of clamping pins and stepped binder together gave better results in terms of WLM/wrinkling prevention and thinning reduction.

It should be noted that the predictions of BHFs combinations are crucial for a successful application of the segmented binder technique. Such predictions can be achieved through analytical or numerical models. For example, He et al. [7] developed a 2-D analytical model to estimate the required BHFs difference for zero weld line movement in a plane strain U-draw-bending process. Kinsey and Cao [8] developed another model to predict WLM given the BHF on both sides which was also extended to predict the required BHF combination required for zero WLM. FE simulations based on reaction forces measured at weld line bonded to the punch were used to estimate the required BHF [9]. Shazly et al. [10] used numerical experiments to study the effect of several variable blank holding force (VBHF) schemes on WLM for a plane strain draw-bending process. Based on the evolution pattern of weld line movements during the drawing process, they suggested applying a higher BHF on the weaker side with its peak value at the beginning of the process. More reduction of the weld line movement was achieved by increasing the peak BHF, however, considerable thinning occurred at the weaker side's wall before complete elimination of the WLM. The same authors [11] also used the reaction forces at the weld line (following Kinsey and Cao [3] and Kinsey et al. [9]) to improve the VBHF scheme.

As shown above, previous analyses are based on the assumption that WLM elimination and thinning reduction

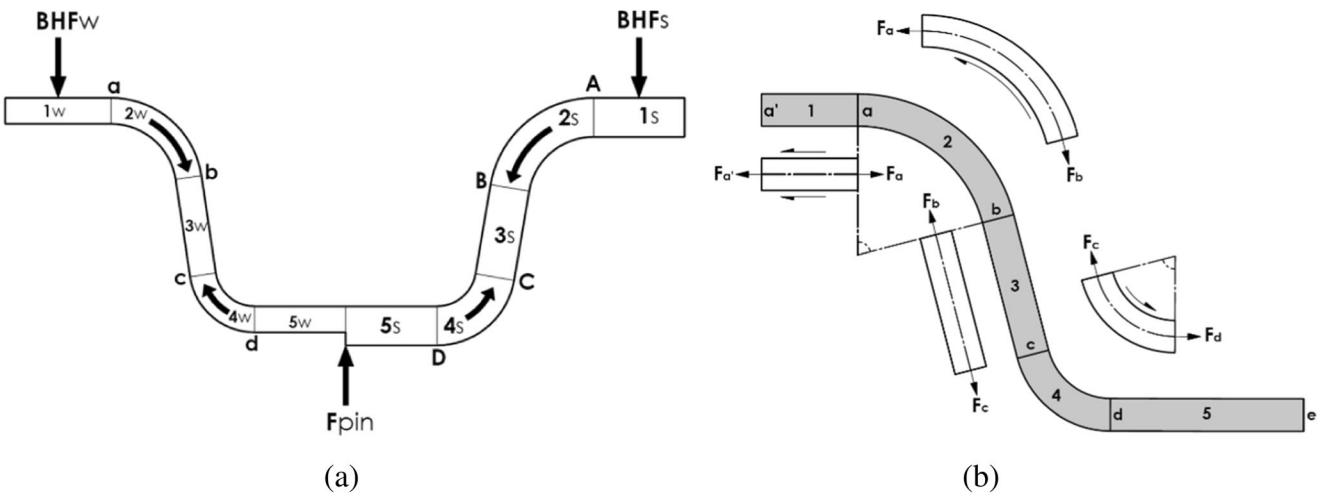

Fig. 1 Draw bending of U-shaped part. **a** Material flow pattern. **b** Profile segmentation for each side

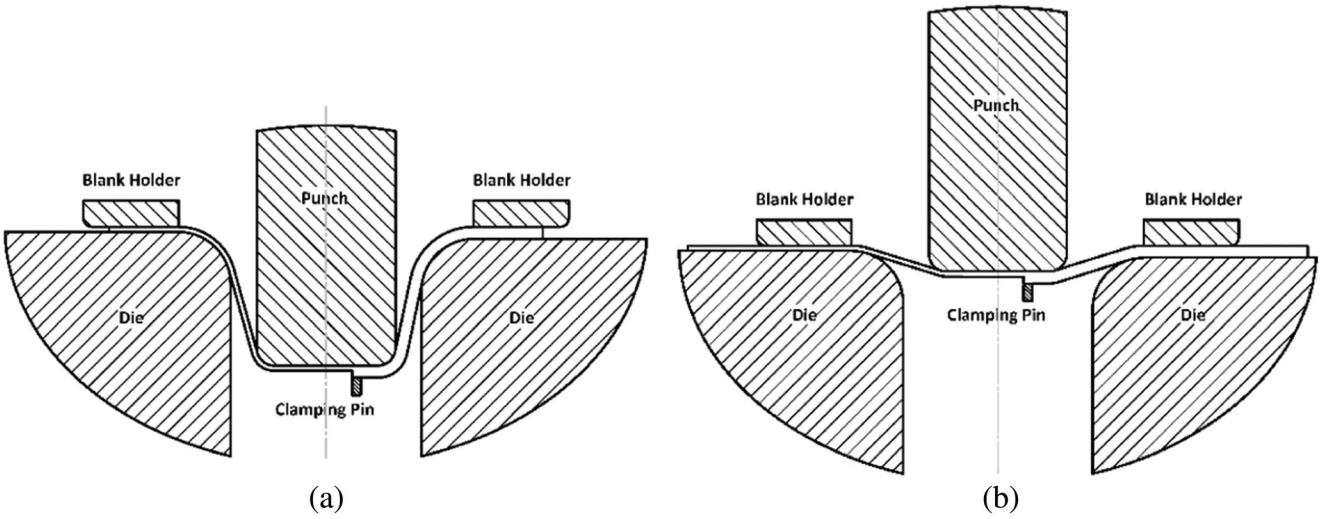

Fig. 2 Blank holding configurations. **a** Case 1: The flange is completely under binder with decreasing blank holding area. **b** Case 2: The flange is partially constrained with a constant blank holding area

are connected. The previous attempts to reduce thinning were done through the elimination of WLM. However, the success of such assumptions depends on the technique used to eliminate WLM. Previous attempts to control the weld line via segmented blank holders only showed significant increase in thinning as a result of increased binding force on the weaker side of the TWB [2, 10]. Alternatively, the clamping pin and counter punch techniques were able to eliminate the WLM without increasing thinning. However, the weaker side showed larger thickness reduction as compared to the stronger side when both are subjected to same BHF. In case of high difference ratio (i.e., thickness and/or strength) between the parent sheets, applying identical BHF may cause tearing at the weaker side and/or wrinkling at the stronger side. In such a case, controlling the weld line by any of the discussed techniques separately will not prevent failure.

In the present work, a 2-D analytical model is developed for a new scheme that combines the segmented blank holder and the clamping pin techniques to control the stretching forces acting on each parent sheet separately such that the tearing limit for each sheet is not exceeded. The scheme is developed and applied on U-shaped drawn parts and extended to box-shaped drawn parts. Given the tool/blank geometry, materials properties, and the BHF on one side, the model provides the required BHF on the other side to produce equal elongation in both sides and calculates the required counter pin force at the weld line to achieve force equilibrium and produce zero WLM. The suggested approach is verified experimentally by a series of laboratory tests under different conditions. Additional experiments on box-shaped parts and finite element tests based on published experimental work from literature are used to demonstrate the advantage of the combined segmented blank holder/counter pin technique over other techniques. The work methodology and model development are presented in the subsequent sections followed by results and discussions.

2 Methodology

2.1 Model development

Considering the schematic drawing in Fig. 1a, if the forces BHF_s, BHF_w, and F_{pin} are to cause identical elongation in both sides, the boundary line between both sides remains fixed horizontally and the flow pattern will be as shown in Fig. 1a. In the present analysis, the friction model $\dot{f} = fe^{\mu\theta}$ is used to describe sliding over the punch/die corners [12], where f is the tensile force normal to the cross section. Side walls are assumed straight and the maximum principal direction is assumed along the deformed shape. The profile of the blank

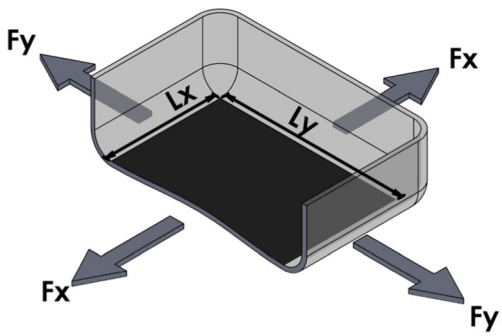

Fig. 3 Biaxial condition at the bottom section—one side of the TWB is illustrated

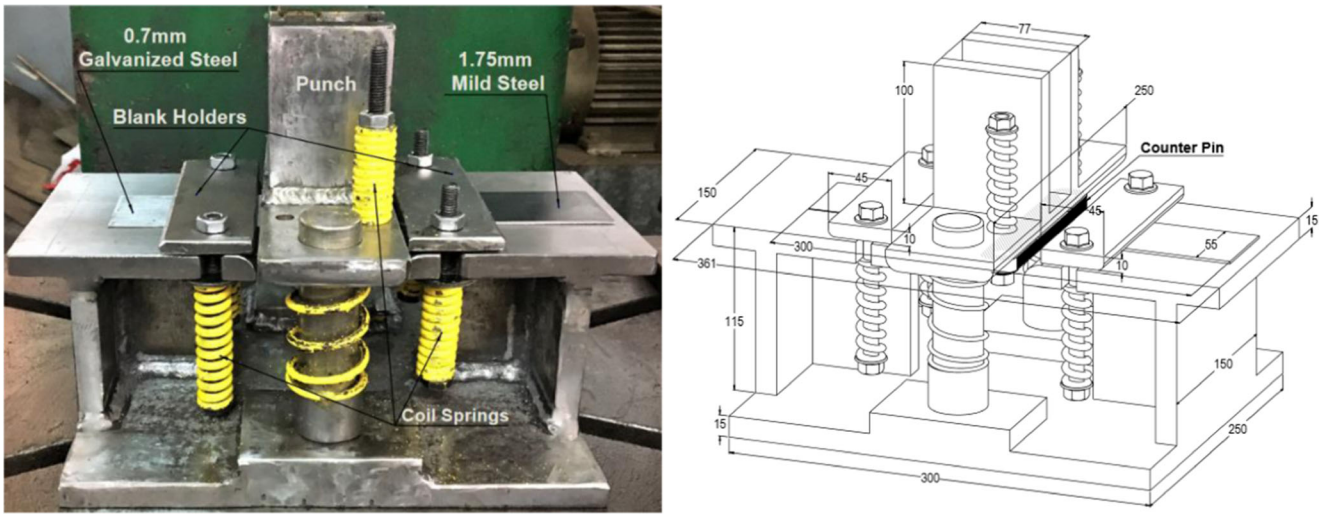

Fig. 4 Assembly and dimensions of the die set used in the experimental work

during the process is divided into ten segments; five segments at each side as shown in Fig. 1b. BHF_s, BHF_w, and F_{pin} are the blank holding force on the stronger side, the weaker side, and the total counter pin force, respectively. The subscripts 's' and 'w' indicate the strong and weak sides. In this model, the clamping pins only contacts the lower face of the blank pushing it against the punch bottom face (i.e. counter pins) [6]. In order to identify the weak and strong sides for a given—initial—thickness/length and material combinations, the elongations for both sides are calculated for a given tensile force F and the side with lower strain and hence elongation will be considered the stronger side. Hence

$$\therefore \Delta L_s < \Delta L_w \quad ; \quad \Delta L = L_o\left(e^{\left(\frac{F}{t_o K}\right)^{\frac{1}{n}}} - 1\right) \tag{1}$$

The tensile forces at the boundaries between segments are obtained from force equilibrium in terms of the blank holding forces as follows:

$$f_a = 2\mu_w(BHF_w), \quad f_A = 2\mu_s(BHF_s) \tag{2}$$

$$f_b = 2\mu_w(BHF_w)e^{\mu_w\theta_w} = f_c, \quad f_B = 2\mu_s(BHF_s)e^{\mu_s\theta_s} = f_C \tag{3}$$

$$f_d = 2\mu_w(BHF_w), \quad f_D = 2\mu_s(BHF_s) \tag{4}$$

The clamping force required to produce frictional forces that eliminate the net horizontal forces and achieve equilibrium at the weld line (not the total clamping force F_{pin}) is given by:

$$F = 2\left(\frac{\mu_s(BHF_s) - \mu_w(BHF_w)}{\mu_p}\right) \tag{5}$$

where μ_p, μ_s, and μ_w are the friction coefficients at the weld line, the strong side and the weak side, respectively. The logarithmic strains along segments 1, 3, and 5 are assumed constant for each segment and are obtained by solving Eq. (6):

$$f = \sigma\, t = K\,(\epsilon\,)^n t_o e^{-\epsilon} \tag{6}$$

where K is the strength coefficient (in the maximum principal direction). The logarithmic strain at the curved segments are averaged as shown in Eqs. (7) and (8):

$$\epsilon_{2w} = \frac{\epsilon_{1w} + \epsilon_{3w}}{2}, \quad \epsilon_{2s} = \frac{\epsilon_{1s} + \epsilon_{3s}}{2} \tag{7}$$

$$\epsilon_{4w} = \frac{\epsilon_{3w} + \epsilon_{5w}}{2}, \quad \epsilon_{4s} = \frac{\epsilon_{3s} + \epsilon_{5s}}{2} \tag{8}$$

The elongation in each segment is calculated from the logarithmic strain in terms of the current length as shown in Eq. (9):

$$\epsilon = \ln\left(\frac{L}{L_o}\right) = \ln\left(\frac{L}{L - \Delta L}\right) \rightarrow \Delta L = L(1 - e^{-\epsilon}) \tag{9}$$

where L and L_0 are the current deformed and original lengths of the segment, respectively. Regardless of the difference in the initial lengths, the target of the model is to provide the BHFs that produce identical elongation for both sides such that:

$$\Delta L_{s_{tot}} = \Delta L_{w_{tot}} \tag{10}$$

where $\Delta L_{s_{tot}}$ and $\Delta L_{w_{tot}}$ are the total increase of the original length (the total elongation) of the strong and weak sides of the TWB, respectively. Knowing that the total elongation is the summation of the segments' elongations in each side, Eq.

Table 1 Characteristics of the TWB used in the present work

Material	Mild steel	Galvanized steel
Thickness (mm)	1.75	0.7
Length (mm)	150	150
Width (mm)	55	55
Yield strength (MPa)	262	233
Tensile strength (MPa)	309	295
n	0.09	0.12
K (MPa)	462	420

(10) becomes:

$$\sum_{i=1}^{5} \Delta L_{is} - \sum_{i=1}^{5} \Delta L_{iw} = 0 \tag{11}$$

Substituting Eq. (9) in Eq. (11) yields

$$\therefore \sum_{i=1}^{5} L_{is}(1-e^{-\epsilon_{is}}) - \sum_{i=1}^{5} L_{iw}(1-e^{-\epsilon_{iw}}) = 0 \tag{12}$$

The current length of segment 1 is obtained in terms of the other segments' lengths for two cases depending on the blank holding area. The first case is illustrated in Fig. 2a, where the flange is completely constrained by the blank holder and the binding area is gradually decreasing with the condition ($L_{BH} \geq L_1$) satisfied. The current length of segment 1 in this case is calculated as follows:

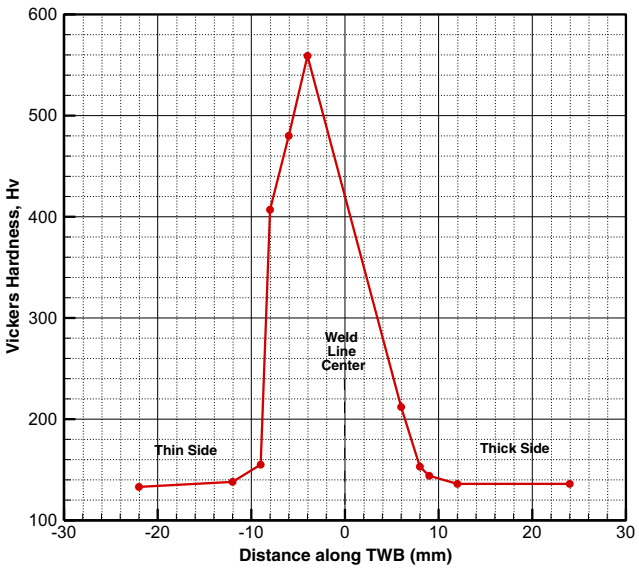

Fig. 5 Vickers hardiness test—HAZ width = 17 mm

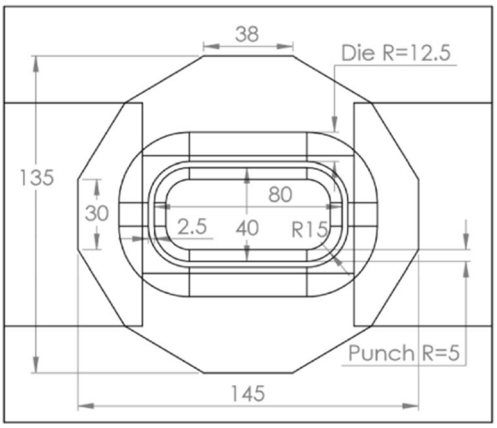

Fig. 6 Dimensions of die set and initial blank used for rectangular box studies in the present analysis. All dimensions in mm

$$\begin{aligned} L_{tot} &= L_{o_{tot}} + \Delta L_{tot} \\ \sum_{i=2}^{5} L_i + L_1 &= L_{o_{tot}} + \sum_{i=2}^{5} L_i(1-e^{-\epsilon_i}) + L_1(1-e^{-\epsilon_1}) \\ \therefore L_1 &= e^{\epsilon_1}\left(L_{o_{tot}} - \sum_{i=2}^{5} L_i e^{-\epsilon_i}\right) \end{aligned} \tag{13}$$

Substituting Eq. (13) in Eq. (12) yields:

$$\begin{aligned} &\therefore \left(L_{ostot}(e^{\epsilon_{1s}}-1) + \sum_{i=2}^{5} L_{is}\left(1-e^{(\epsilon_{1s}-\epsilon_{is})}\right)\right) \\ &-\left(L_{owtot}(e^{\epsilon_{1w}}-1) + \sum_{i=2}^{5} L_{iw}\left(1-e^{(\epsilon_{1w}-\epsilon_{iw})}\right)\right) = 0 \end{aligned} \tag{14}$$

The second case is illustrated in Fig. 2b, where the binding area is kept constant by constraining a specific domain in the flange. In this case, the flange is divided into two segments; one is under the binder segment (L_1 = blank holder contact length) and the other is the unconstrained segment ($L_{1'} \geq 0$) which gradually decreases with the punch movement. When the length of segment $L_{1'}$ becomes zero, case 1 is then

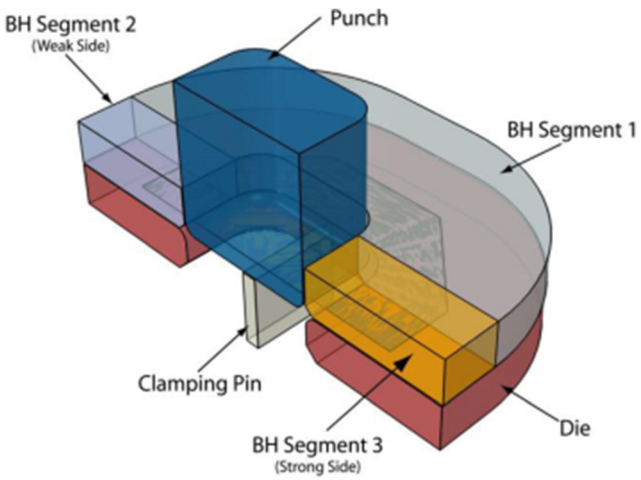

Fig. 7 Half the die set for the proposed approach

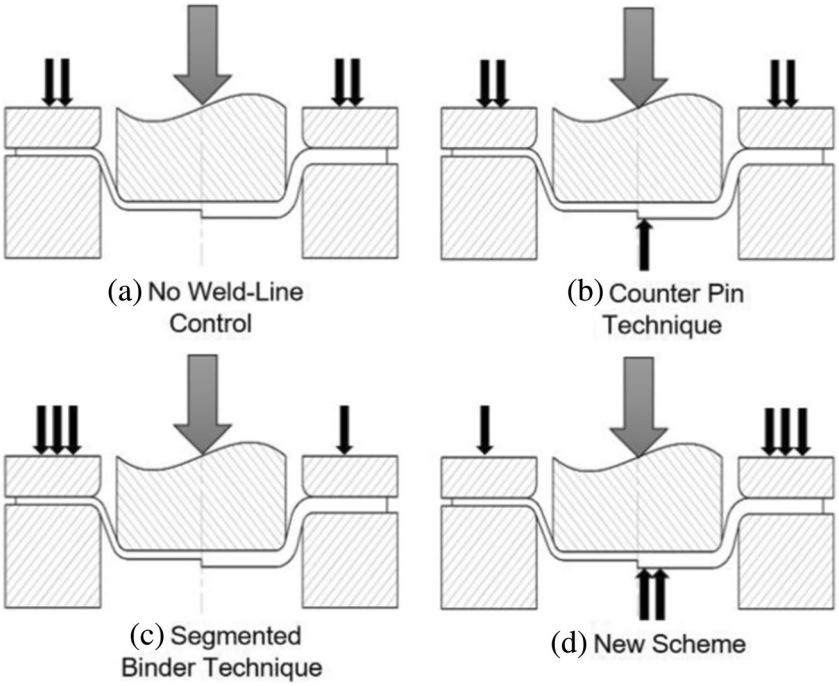

Fig. 8 Schematics for each of the compared WLM controlling schemes

retrieved. The length of segment $L_{1'}$ is calculated as follows:

$$\begin{aligned} L_{\text{tot}} &= L_{o_{\text{tot}}} + \Delta L_{\text{tot}} \\ \sum_{i=1}^{5} L_i + L_{1'} &= L_{o_{\text{tot}}} + \sum_{i=1}^{5} L_i(1-e^{-\epsilon_i}) \\ \therefore L_{1'} &= L_{o_{\text{tot}}} - \sum_{i=1}^{5} L_i e^{-\epsilon_i} \end{aligned} \tag{15}$$

The current lengths of segments 2, 3, 4, and 5 are calculated using the geometrical model (see Appendix A for details) with respect to the current position of the punch such that:

$$L_{2\text{w}} = \theta_{\text{w}} R_{\text{dw}}, \qquad L_{2\text{s}} = \theta_{\text{s}} R_{\text{ds}} \tag{16}$$

$$L_{4\text{w}} = \theta_{\text{w}} R_{\text{pw}}, \qquad L_{4\text{s}} = \theta_{\text{s}} R_{\text{ps}} \tag{17}$$

$$L_{3\text{w}} = \frac{Y - T_{\text{w}}(1-\cos\theta_{\text{w}})}{sin\theta_{\text{w}}} \quad , \quad L_{3\text{s}} = \frac{Y - T_{\text{s}}(1-\cos\theta_{\text{s}})}{\sin\theta_{\text{s}}} \tag{18}$$

The wrap angle is related to the punch vertical displacement as follows:

$$\begin{aligned} \theta &= 2\tan^{-1}\left(\frac{C-\sqrt{C^2+Y^2-2TY}}{2T-Y}\right); Y \neq 2T \\ C &= c + R_{\text{p}} + R_{\text{d}}, \qquad T = t + R_{\text{p}} + R_{\text{d}} \end{aligned} \tag{19}$$

In order to eliminate the effect of internal bending moments M_{s} and M_{w} at segments 4_{s} and 4_{w}, which contribute to the vertical WLM and reduce the resultant counter pin force (F_{pin}), additional amount of force F' must be applied by the counter pin such that:

$$\begin{aligned} F' &= \frac{M_{\text{s}}}{L_{5\text{s}}} + \frac{M_{\text{w}}}{L_{5\text{w}}}; \quad where\ M \\ &= 2\int_{r=0}^{r=0.5t} rK\left(\ln\left(1+\frac{r}{R+0.5t}\right)\right)^n dr \quad ; \\ R &= R_{\text{p}} \end{aligned} \tag{20}$$

The bending moment is calculated assuming the neutral line at the mid-plane of the sheet and neglecting the effect of stretching (see Appendix A). Moment integration is done numerically and the total minimum counter pin force is then calculated as:

$$F_{\text{pin}} = F + F' \tag{21}$$

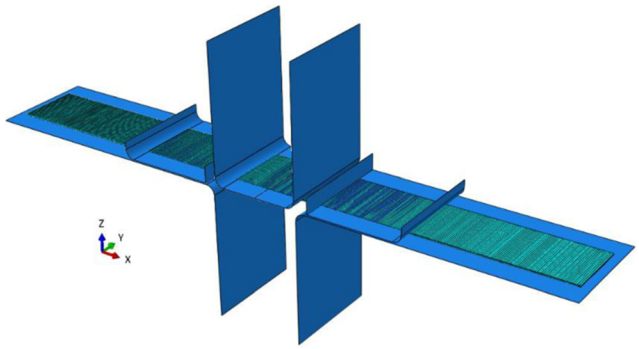

Fig. 9 FEA model for plane strain draw-bending process based on refs. [13, 14]

Table 2 Input values the selected case studies

Case Configuration	Case1		Case2		Case3		Case4		Case5		Case6		Case7	
	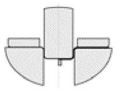		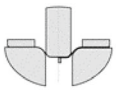		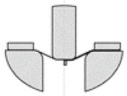		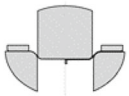		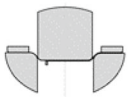		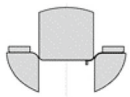		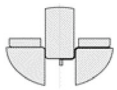	
Thickness ratio t_{ow}/t_{os}	0.25		0.25		0.25		0.25		0.25		0.25		1/12	
Original Sheet Length (*Lw/Ls*)	1		1		1		1		5/9		9/5		1	
Punch Corner Radius (*Rp*)	$10t_{ow}$	$10t_{ow}$	$20t_{ow}$	$20t_{ow}$	$20t_{ow}$	$20t_{ow}$	$20t_{ow}$	$20t_{ow}$	$20t_{ow}$	$20t_{ow}$	$20t_{ow}$	$20t_{ow}$	$20t_{ow}$	$20t_{ow}$
Die Corner Radius (*Rd*)	$10t_{ow}$	$10t_{ow}$	$40t_{ow}$	$40t_{ow}$	$40t_{ow}$	$40t_{ow}$	$40t_{ow}$	$40t_{ow}$	$40t_{ow}$	$40t_{ow}$	$40t_{ow}$	$40t_{ow}$	$20t_{ow}$	$20t_{ow}$
Punch Die Clearance (*c*)	$2t_{ow}$	$6t_{ow}$	$2t_{ow}$	$6t_{ow}$	$40t_{ow}$	$40t_{ow}$	$2t_{ow}$	$6t_{ow}$	$2t_{ow}$	$6t_{ow}$	$2t_{ow}$	$6t_{ow}$	$20t_{ow}$	$20t_{ow}$
Punch Face Width (*P*)	$100t_{ow}$		$100t_{ow}$		$100t_{ow}$		$280t_{ow}$		$280t_{ow}$		$280t_{ow}$		$100t_{ow}$	
Initial Weld Line Position (*Xw*)	*0*		*0*		*0*		*0*		*-100t_{ow}*		*+100t_{ow}*		*0*	
BHFs	Minimum value to prevent the sheet from departing the die													

In box-shaped drawing, the straight sides can be approximated by 2-D plane strain sections, while the bottom section at the punch face is subjected to biaxial stretching forces as shown in Fig. 3.

Assuming the weld line is along direction "y," the elongation in direction "x" at the bottom in each side is:

$$\Delta L_x = L\left(1-e^{-\epsilon_x}\right)$$

Equation (6) then becomes:

$$F_x = \frac{\left(\epsilon_x\sqrt{\frac{4}{3}\left(1+\beta+\beta^2\right)}\right)^n}{\sqrt{1-\alpha+\alpha^2}} \times K\, t_o e^{-(1+\beta)\epsilon_x} \tag{22}$$

where $\alpha = \frac{\frac{F_y}{L_x}}{\frac{F_x}{L_y}}$, $\beta = \frac{2\alpha+1}{2+\alpha}$

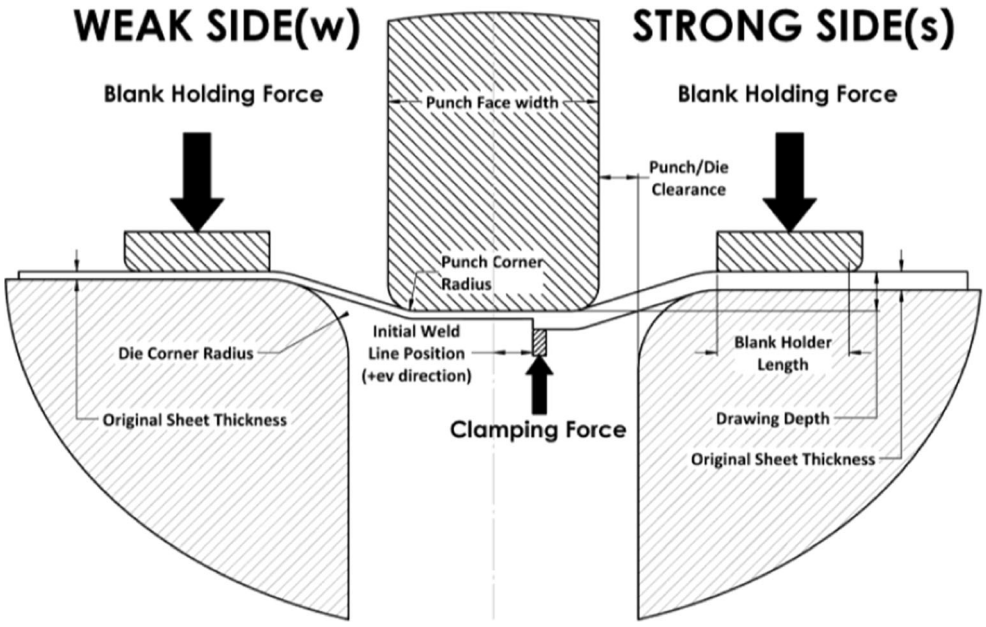

Fig. 10 Draw-bending process for all cases with process and geometrical input parameters

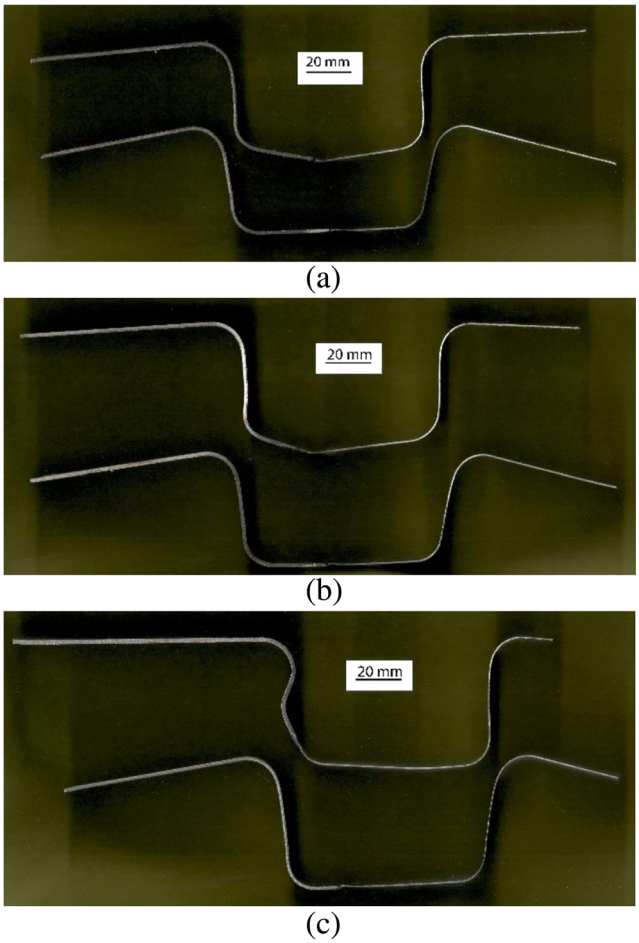

Fig. 11 Experimental comparisons between free weld line and new scheme. **a** Cases A and D. **b** Cases B and E. **c** Cases C and F

2.2 Model verification

2.2.1 U-draw-bending model

Laboratory experiments are conducted to verify the developed analytical model and prove its feasibility in practice. The die set assembly shown in Fig. 4 is used to conduct U-draw-bending experiments on TWBs. In the present work, a TWB consisting of a mild and galvanized steel parent sheets are TIG welded prior to drawing. The geometrical and material properties of the parent sheets are measured and given in Table 1. The width of the heat affected zone (HAZ) is obtained via HV-50A Vickers hardness tester as shown in Fig. 5. The HAZ width is found to be approximately 17 mm, with 8 mm on the thicker side and 9 mm on the thinner side. A strength coefficient and hardening exponent of 355 MPa and 0.173, respectively, are obtained from a tension test specimen of the HAZ.

The BHF and the counter-pin force are applied using two coil compression springs with identical stiffness of 70 N/mm on each side. Six different experiments with different conditions are used to verify the analytical model. In the first three experiments namely cases A, B, and C, the weld line is initially shifted from the center of the punch toward the thicker side by 0, 10, and 20 mm, respectively. Both sides are subjected to identical BHF of 3080 N and no direct constrain at the weld line. The value of this force is the minimum required for successful drawing and was determined by FE simulations. The friction coefficients for the parent sheets are taken initially as 0.2 for the mild steel and 0.17 for galvanized steel and are used to simulate one of the cases (e.g., case C) using ABAQUS/Explicit. These values are then adjusted such that the total elongation, WLM, and the final deformed shape for simulation and experiment are identical. The adjusted friction coefficient values are then used in the analytical model to generate the required BHF and counter punch force that will be applied to cases D, E, and F to achieve identical elongation in both sides and zero WLM. Cases D, E, and F share the same initial weld line position as cases A, B, and C, respectively, while the weld line is constrained by a counter pin. The experimental results of these six cases are presented in "Section 3."

2.2.2 Box-shaped drawn model

The extended analytical model for box shape is used to apply the combined segmented binder/counter-pin

Table 3 Experimental and FE results for model verification

Case no.	Weld line position (mm)	BHFw/BHFs	Fpin/BHFs	*Lw*/*Ls*	HWLM (mm)	VWLM (mm)
A (experiment)	0	1.00	0.0	1.013	7.4	5.1
B (experiment)	10	1.00	0.0	1.020	13.8	5.6
C (experiment)	20	1.00	0.0	1.020	20.0	11.2
C (simulation with HAZ)	20	1.00	0.0	1.014	19.2	11.3
C (simulation without HAZ)	20	1.00	0.0	1.019	19.4	11.4
D (experiment)	0	0.13	1.1	1.001	0.0	0.0
E (experiment)	10	0.13	1.2	1.000	0.0	0.0
F (experiment)	20	0.13	1.5	1.007	0.0	0.0

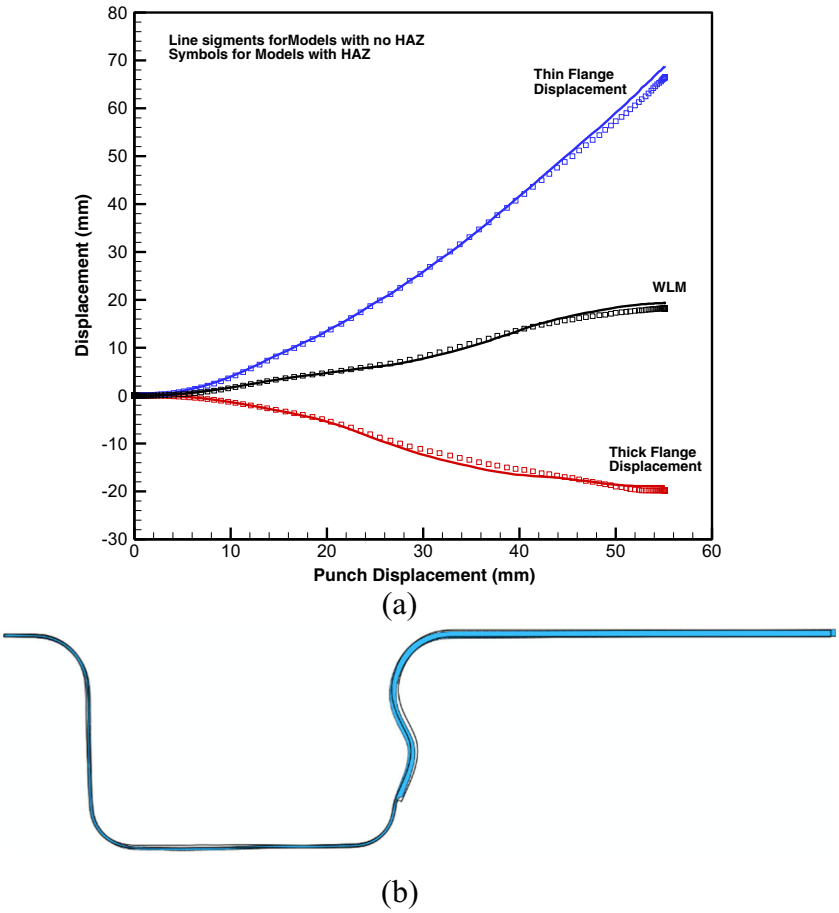

Fig. 12 Comparisons between FE models with and without HAZ for case 3. **a** Flange displacement and WLM. **b** Overlay plot of the drawn parts—line model for FE model with HAZ

technique to the TWB of rectangular box-shaped parts produced by the die set shown in Fig. 6. The experimental setup shown in Fig. 4 is upgraded to accommodate the dimensions of the rectangular box shown in Fig. 6 with segmented binder/counter pin as schematically shown in Fig. 7. The TWB used in the rectangular box-shaped parts consists of a 2-mm low carbon steel sheet with a strength coefficient and a hardening exponent of $K = 436$ MPa and $n = 0.38$, respectively, and a 1-mm low carbon steel sheet with a strength coefficient and a hardening exponent of $K = 509$ MPa and $n = 0.22$, respectively. Three different experiments are conducted to test different conditions. In the first experiment, a base line experiment, the TWB is subjected to identical BHF and the weld line is unconstrained. The objective of this experiment is to determine the limiting drawing height. The second experiment (only counter-pin case) is the same as the first experiment except for the additional clamping of the weld line provided by the counter pin to prevent its movement. In the third experiment (new scheme), the weld line is clamped and the BHF on the weaker and stronger sides and the counter-pin force are determined using the procedure detailed in Appendix B. Finally, a finite element model is constructed and validated following the data of the experimental work reported by Morishita et al. [4] to compare the proposed scheme against the counter punch technique. The developed analytical model in the present work is applied to

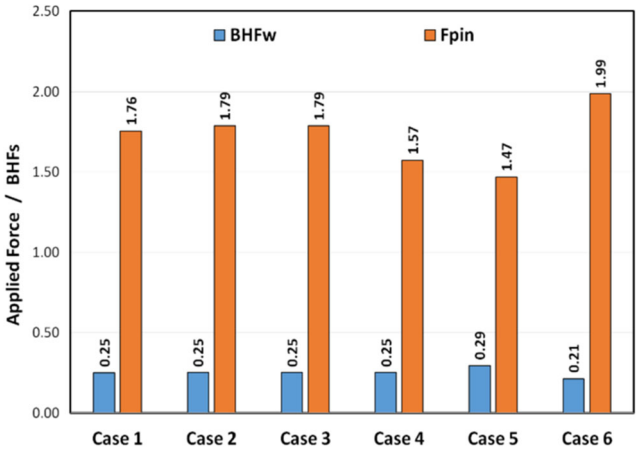

Fig. 13 Forces predicted by the developed analytical model in each case and used in the FE simulations

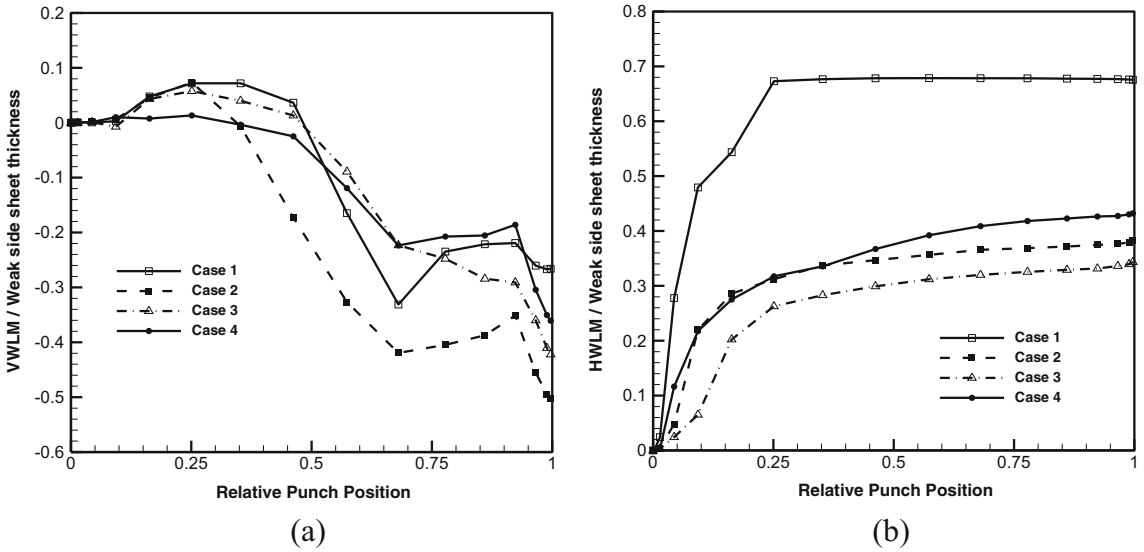

Fig. 14 Weld line movement relative to punch position. **a** Vertical (VWLM). **b** Horizontal (HWLM)

the validated FE model to test its merit in drawing square box-shaped part. The selected case consists of a TWB made of two mild steel sheets with thickness ratio of 0.6/1.16 mm. Detailed die design and process parameters can be found in ref. [4]. The blank is simulated using four node reduced integration shell elements with five integration points through thickness and a dynamic explicit step of 0.01 s to model the forming stage of the TWB. All other parts are modeled as rigid bodies. As reported during the physical experiments, lubrication was used at the flange zone to facilitate the metal flow into the die opening. Therefore, a coulomb friction model with 0.2 and 0.25 friction coefficients are applied to the flange and punch area, respectively. Due to symmetry of the experiment, only half model is considered as shown in Fig. 7.

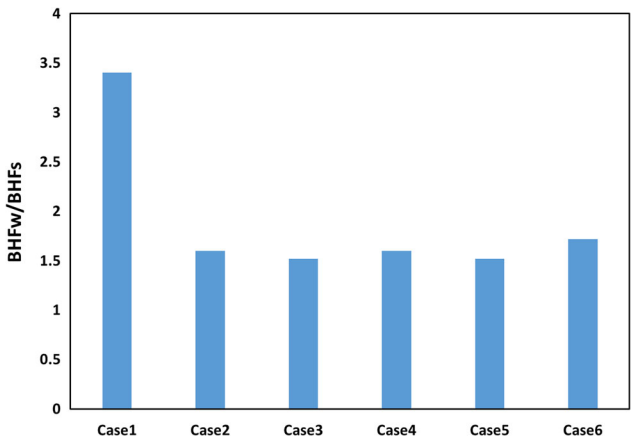

Fig. 15 BHF inputs for the segmented binders technique

2.3 Applications of the combined segmented binder/counter-pin developed scheme to the U-draw-bending process

For the draw-bending process, a comparison between the four schemes shown in Fig. 8 including the proposed scheme is applied using the ABAQUS 6.14 finite element software. A series of 24 (six for each technique in Fig. 8) simulations based on the plane strain draw-bending benchmark test of a homogenous blank reported by Taylor et al. [13] are carried out in this section. The original benchmark test is used for verification in "ABAQUS Documentations" [14]. Considering the homogenous blank as a special case of TWBs with neglected weld line and identical parent sheets, the FE model is reproduced for the comparison as shown in Fig. 9. The insignificance of the weld line in TWBs forming simulation is discussed by Zhao et al. [15] and tested in "Section 3." All model data such as geometry, materials' properties, and friction conditions can be found in ref. [14]. The same element size as the benchmark problem [14] is adopted here and has been verified by comparisons with other sizes. The recorded spring back angle between the flange and the horizontal line in the produced model is 0.22 rad and the experimental measurements range from 0.16 to 0.4 rad (avg. = 0.28 rad).

All model parameters in the FE model are kept constant except for the necessary tooling parameters and the applied force schemes. The BHF at the strong side is kept as applied in the benchmark test as well as the other side except for the schemes where different force schemes applies. A mild steel blank shown in Fig. 9 with thicknesses ratio (t_{ow}/t_{os}) of 0.25 is used for all cases in Table 2 expect

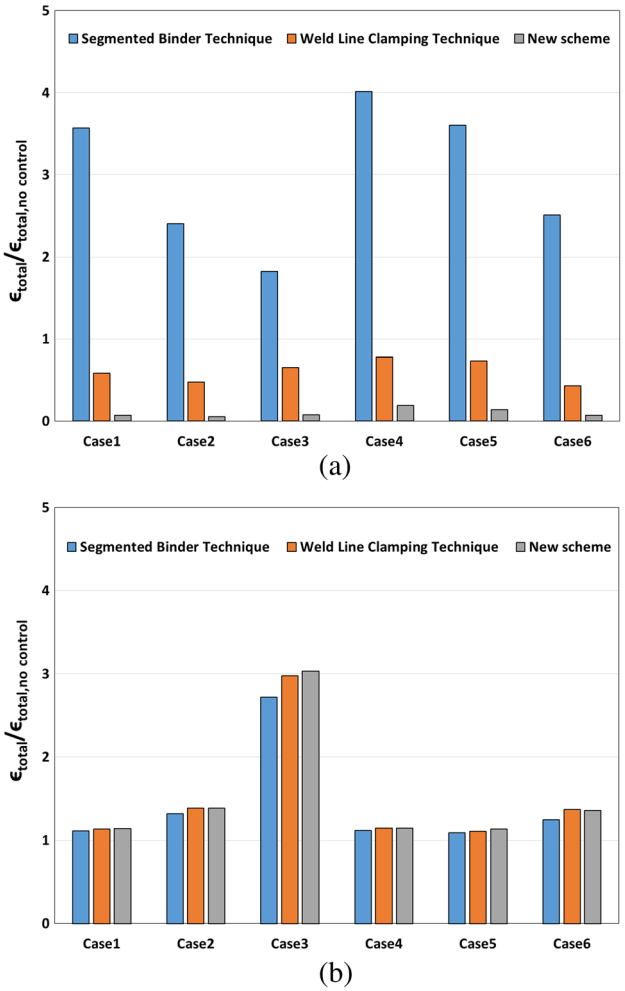

Fig. 16 Normalized overall thinning strain. **a** Weaker side. **b** Stronger side

for case 7. Cases 1, 2, and 3 have the same blank geometry but different tool geometrical parameters and cases 4, 5, and 6 share the same tool geometry but different blank geometry. Figure 10 shows schematically the blank, TWB holder, and die assembly with the geometrical and process parameters assigned to each part. For each of the first six cases, the blank/tool geometry, the material properties, the friction coefficients, and a selected value of the BHF on the strong side are inserted to the analytical model. The resulting BHF on the weak side and the counter-pin force (clamping force) at the weld line are inserted to the FE model.

In case 7, the comparison is extended to extreme limits where a 1/12 thickness ratio and 0.4 friction coefficient are selected to present a case in which, applying identical BHF on both sides will cause tearing at the weaker side and incomplete bending (or wrinkling) at the stronger side. In such case, increasing the BHF on the weaker flange or reducing the BHF on the stronger side is not justified; thus, the segmented binders technique is excluded from the comparison in case 7.

3 Results and discussions

3.1 Draw-bending process

Figure 11 shows the parts produced under U-draw-bending process for cases A to F. These figures are used to extract the total elongation of each side for all cases. As shown in Table 3 and Fig. 11, the elongation ratio is close to unity and the WLM is eliminated in cases D, E, and F as targeted by the analytical model.

The experimental work is also used to investigate the significance of incorporating HAZ properties into the FE model. As shown in Table 3, the final elongation and WLM for case C for two FE models; with and without HAZ, agree well with the measured experimental results. The flange draw-in and WLM for both FE models are shown in Fig. 12a while an overlay plot for the two models is shown in Fig. 12b. The simulation results show good agreements between the FE models developed with and without considering modeling HAZ. This indicates that modeling HAZ has no impact on TWB drawn parts as also suggested by Zhao et al. [15].

The same analytical model is solved to apply the proposed scheme to each of the cases listed in Table 2. Figure 13 shows the calculated BHF_w and the counter pin forces (F_{pin}) required for cases 1 to 6. Figure 14 shows the vertical WLM and horizontal WLM resulted from applying the new scheme for these cases.

The blank in cases 1 to 4 has the same original dimensions and thus the predicted values of BHF_w and F_{pin} are close to each other except for case 4. In case 4, the length of segments L_{5s} and L_{5w} at the punch face are much larger than cases 1, 2, and 3, such that less forces are required to overcome the internal bending moment at segments L_{4s} and L_{4w}. In case 5, the thicker side is extended by 28.5% more than the thicker side of case 4. At the same time, the thinner side is shortened by 28.5% less than the thinner side of case 4 such that the BHF_w applied in case 4 will produce less elongation in the thinner side of case 5. Consequently, the calculated BHF_w in case 5 is higher than case 4 in order to overcome the shortage at the thinner side and the additional elongation at the thicker side while the F_{pin} is decreased to maintain force equilibrium along the blank profile. The modifications applied in case 6 are the opposite of those applied to case 5, thus the analytical model predicts less BHF_w and higher F_{pin} in case 6 as compared to case 4.

The six cases are used for comparisons between the four schemes shown in Fig. 8. The proper BHF combination for the segmented binder technique that leads to zero WLM is obtained by a matching procedure (see Appendix B) and shown in Fig. 15. For the weld line clamping technique, displacement

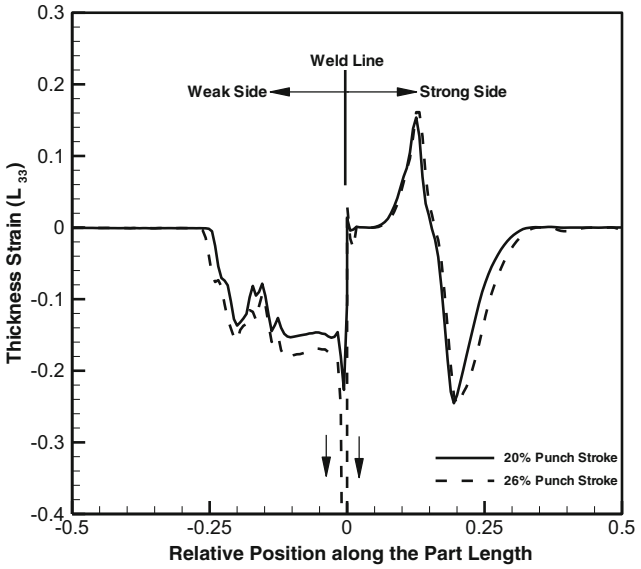

Fig. 17 Thickness strain along the blank top surface at different punch depths—uncontrolled condition

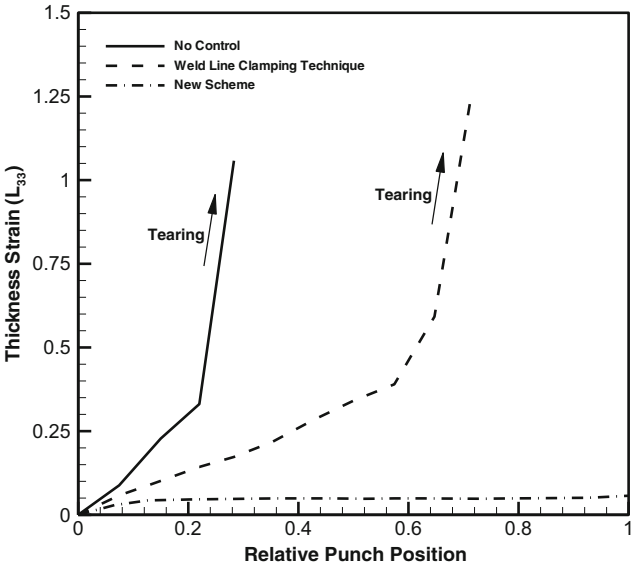

Fig. 19 Maximum absolute thickness strain at the weaker side at different punch positions

constrains are applied to the weld line such that no WLM occurs. For each case, the final deformed lengths (L) at the top and bottom surfaces are extracted from FE models to calculate an average total (overall) tensile strain in each side as follows:

$$\epsilon_{total} = \ln\frac{L}{L_o}, \quad L = \frac{L_{\text{top surface}} + L_{\text{bottom surface}}}{2} \tag{23}$$

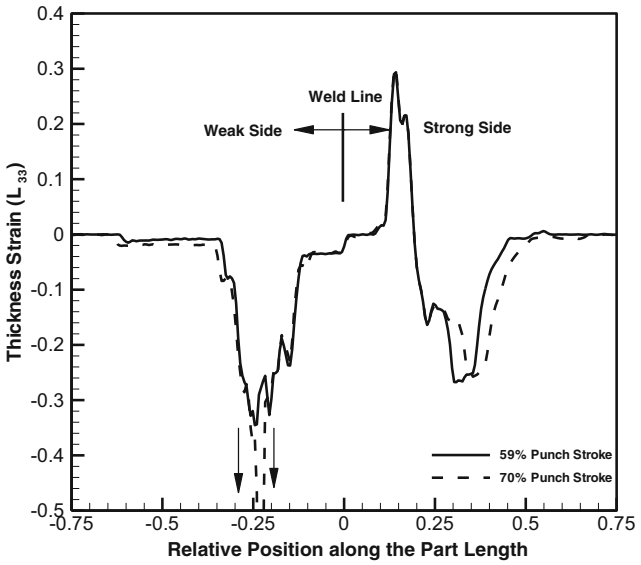

Fig. 18 Thickness strain along the blank top surface at different punch depths—Weld line clamping technique

Recalling the plane strain condition, the average tensile strain can be used as an indication of the overall thinning in each side of the deformed blank. For the sake of comparison, the overall thinning strain value for each of the three schemes b, c, and d shown in Fig. 8 is divided by the strain value of scheme a for the same case. A value higher than one indicates that the applied technique causes more thinning compared to the uncontrolled condition and vice versa.

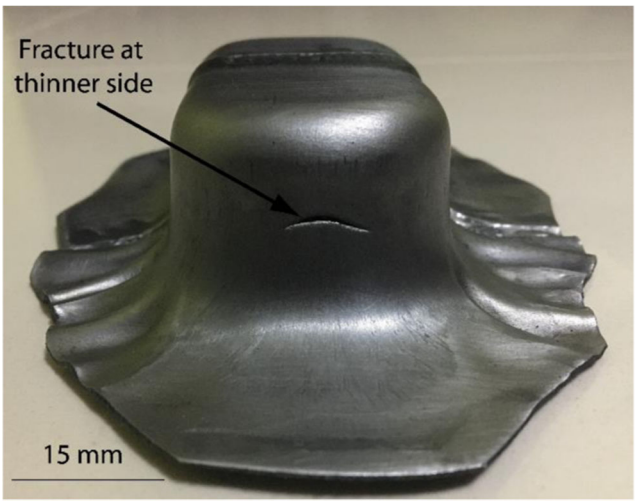

Fig. 20 Rectangular drawn box with no counter pin and equal BHF

Fig. 21 Rectangular drawn box using a counter pin and equal BHF and the new scheme

As shown in Fig. 16a, the segmented binder technique causes significant thinning (81 to 274% increase) in the weaker side and consequently decreases the sheet formability. On contrary, the new technique shows considerable reduction in thinning (81.5 to 94.4% decrease) at the weaker side as well as the weld line clamping technique which shows less thinning reduction (21.5 to 57%). Furthermore, the stronger side is hardly affected by any of the discussed techniques in all cases except case 3 as shown in Fig. 16b. In case 3, large punch/die clearance facilitates the sliding of the stronger segment at the punch face to the side walls, resulting in less overall stretching compared to the other three conditions where the stronger side is forced to stretch over the punch corner.

In case 7, the uncontrolled condition is modeled first and the recorded maximum WLM before failure are 13Tw and 30Tw in the horizontal and vertical directions (relative to the punch displacement), respectively. The BHF at the stronger side shows insufficient constraining while the weaker side suffers from early failure near the weld line. Localized necking is observed at 26% punch travel as shown by the thickness strains distribution along the top surface of the blank in Fig. 17. Likewise, application of the weld line clamping technique with identical BHF causes insufficient constraining at the strong side and tearing at the weaker side where localization of necking in the side walls is observed at 70% punch travel as shown in thickness strain distribution in Fig. 18.

On the other hand, when the BHF is decreased on the weaker flange and increased on the stronger flange as the new scheme suggests, a complete punch stroke with no failure is obtained as shown in Fig. 19 where a comparison of the maximum thinning strain (absolute value) at different punch positions is presented for the three models. The new scheme (combined segmented binder/counter pin—BHFw/BHFs = 0.085) shows considerable reduction in thinning at the weaker side. In contrast, thinning is considerably high at the two other cases namely the weld line clamping technique (horizontally fixed weld line—BHFw/BHFs = 1) and the uncontrolled condition (free weld line—BHFw/BHFs = 1).

3.2 Rectangular box-shaped drawn parts

Figure 20 shows the drawn rectangular box for the first case with no counter pin and equal BHF. The thinner side fractured at a cup height of 30 mm. Figure 21 shows the drawn rectangular box at cup height of 35 mm for counter-pin case and new scheme. In both cases, the rectangular box is drawn successfully. The drawn parts are then sectioned and the part thicknesses close to the paths shown in Fig. 22 are measured. Figure 23 shows a comparison between the thickness distributions for the counter pin scheme and new scheme. The new scheme showed an improvement in the thickness reduction, especially along 90 and 45 degree paths.

Figure 24 shows a comparison between experimental measurements by Morishita et al. [4], and the FE model developed for the same case. The logarithmic thickness

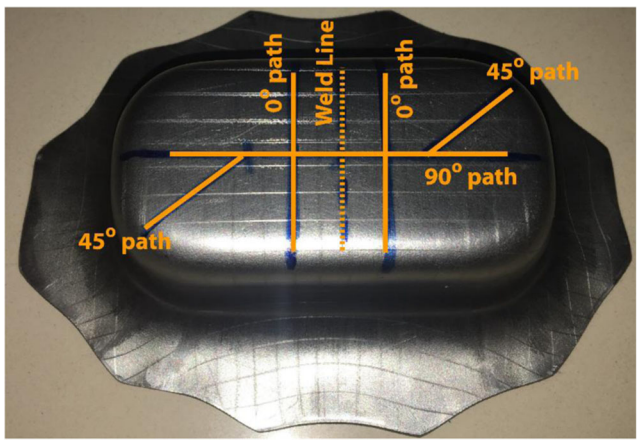

Fig. 22 Path directions for thickness comparisons

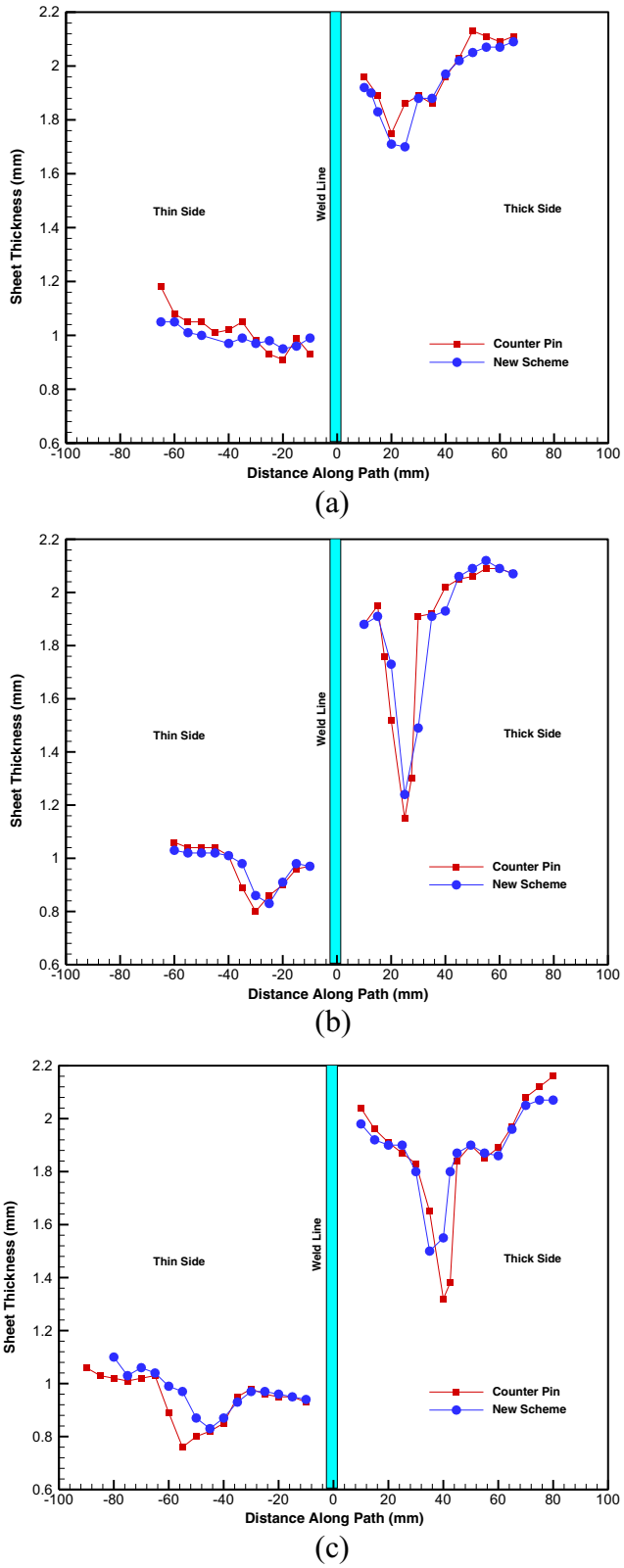

Fig. 23 Thickness distribution for experimental work on rectangular box-shaped drawn parts. **a** 0 degree path. **b** 45 degree path. **c** 90 degree path

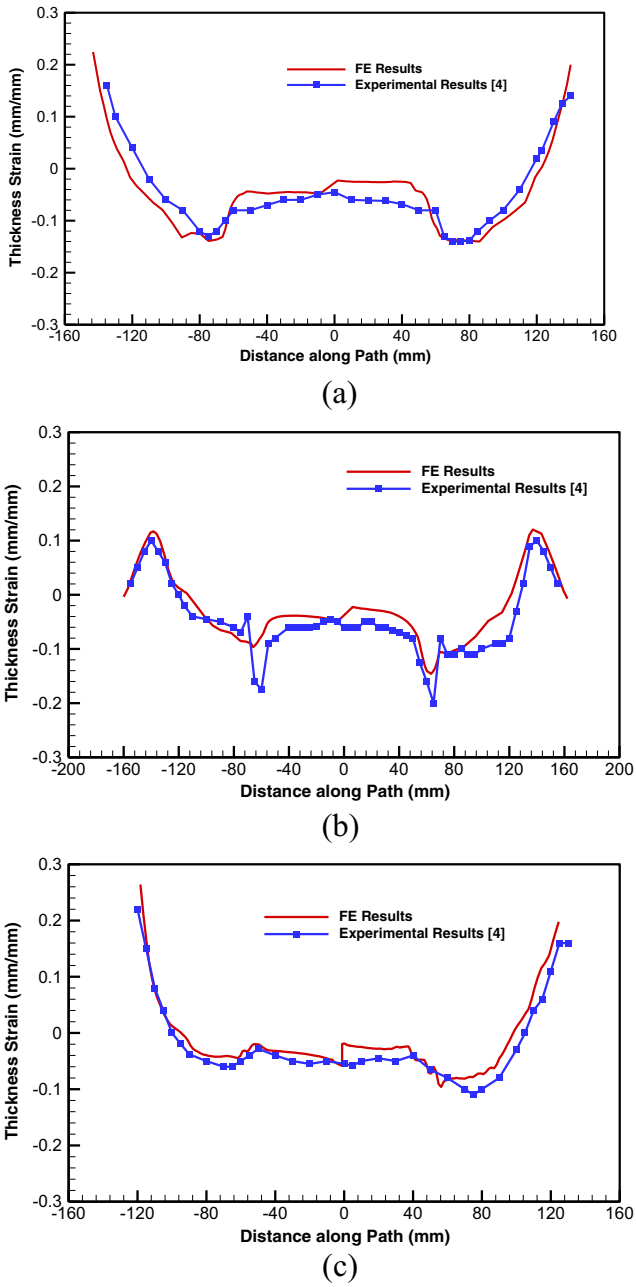

Fig. 24 Thickness strain distribution for experimental work by Morishita et al. [4] and FE simulation along. **a** 0 degree path. **b** 45 degree path. **c** 90 degree path. The thick side is located on the positive *x*-axis

strains along the deformed paths show good agreement to the experimental result and hence validates the FE model. The FE model results of the proposed scheme are shown in Fig. 25. The applied BHFw/BHFs and Fpin/BHFs ratios from the analytical model are 1/2 and 20, respectively. The measured WLM and the final

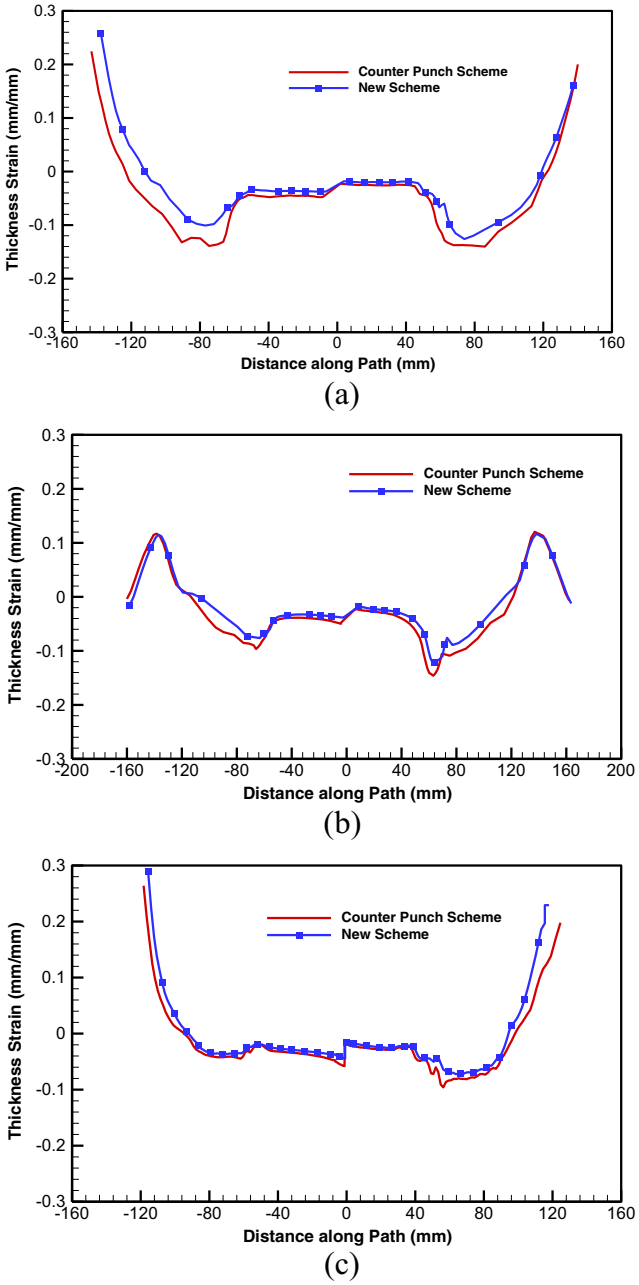

Fig. 25 Thickness strain distribution for FE model based Morishita et al. [4] approach and present scheme. **a** 0 degree path. **b** 45 degree path. **c** 90 degree path. The thick side is located on the positive *x*-axis

length ratio Lw/Ls from the FE model are 1.19 mm and 1.02 between both sides, respectively. Such slight deviation from the analytical model is affordable considering the considerable thinning reduction (17 to 28% at the corner zone Fig. 24) when the simplified approach is adopted [12]. All attempts to eliminate the WLM or increase the drawing limit using the conventional segmented binder scheme alone in which higher binding force is applied to the stronger side and lower force to the weaker side had failed. Although the application of the conventional segmented binder scheme alone seems to be easier in practical terms, it increases the sheet thinning and reduces the cup drawing limit. The combined segmented binder/counter-pin technique proves to be advantageous over other techniques and show significant reduction in drawn parts.

4 Conclusions

The present work suggested a new binding scheme to reduce the thinning of TWBs. This scheme combined weld line constraining via counter pins while applying a lower BHF on the weaker side as compared to the stronger side via segmented binders to achieve minimum thinning in the final product. Adopting this scheme, an analytical model was developed for the plane strain 2-D draw-bending process to determine the required BHF and counter-pin force values. Laboratory and numerical experiments were conducted to examine the developed analytical model and compare the proposed controlling scheme with other schemes. The experimental results showed that the new scheme was physically applicable and was capable of providing accurate force values that sufficiently eliminate the weld line movement and enhance formability (substantial reduction in thinning).

The present study showed the merit of implementing the proposed scheme in cases where large thickness and/or strength ratio of the sheets comprising the TWB exist. In such cases, conventional segmented binders alone or weld line clamping technique without any variation in the applied BHF at each side cannot prevent failure.

Adopting the simplified approach presented in ref. [12], the study proposed a 3-D binding scheme for the TWB box-shaped parts. Experimental work conducted in deep drawing of rectangular box-shaped parts showed that the new scheme resulted in improvement in thickness reduction in the final product. Furthermore, a comparison with published experimental work using counter punch technique validated the feasibility of applying the proposed binding scheme. Finite element investigations showed a clear improvement in the formability of the considered case study. These results showed the merit of the developed scheme in improving the quality of the drawn box-shaped parts made from TWBs.

Appendix A: Geometrical Model

$$\mathrm{Rd}' = \mathrm{Rd} + \frac{t}{2} \quad [1]$$

$$\mathrm{Rp} = \text{punch radius}, \quad \mathrm{Rp}' = \mathrm{Rp} + \frac{t}{2} \quad [2]$$

$$Y = yp + yd + h$$

$$\text{Let } c' = c - t \qquad [3]$$

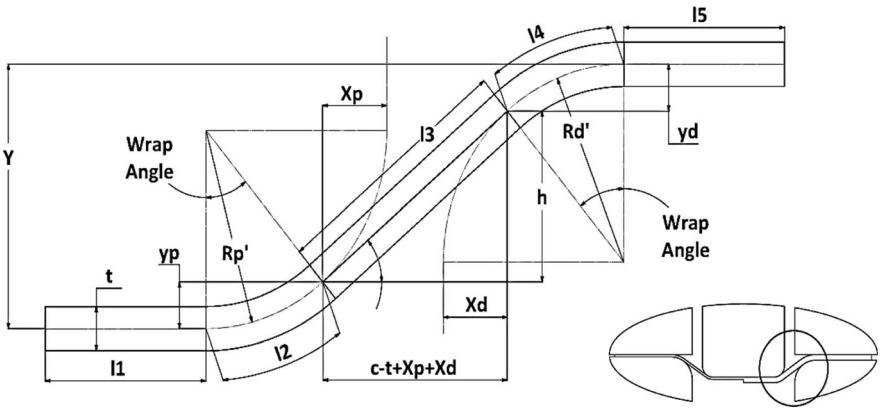

$$xp = Rp'(1-\sin\theta),$$

$$xd = Rd'(1-\sin\theta),$$

$$yp = Rp'(1-\cos\theta),$$

$$yd = Rd'(1-\cos\theta),$$

$$h = (c' + xp + xd)\tan\theta$$

$$\therefore Y = R'p(1-\cos\theta) + R'd(1-\cos\theta) + (c' + R'p(1-\sin\theta) + R'd(1-\sin\theta))\tan\theta$$

Substituting with [1], [2], [3] and rearranging

$$Y = (c + Rp + Rd)\tan\theta - (t + Rp + Rd)(\sec\theta - 1)$$

Using MATLAB built-in solver

$$\theta = 2\tan^{-1}\left(\frac{C - \sqrt{C^2 + Y^2 - 2TY}}{2T - Y}\right); \quad Y \neq 2T$$

$$C = c + R_\mathrm{p} + R_\mathrm{d}; \; T = t + R_\mathrm{p} + R_\mathrm{d}$$

Bending Moment Equation

$$\epsilon = ln\frac{l}{l_o} = ln\frac{\theta(R_p + 0.5t + r)}{\theta(R_p + 0.5t)} = ln\left(1 + \frac{r}{R_p + 0.5t}\right)$$

$$M = 2\int_{r=0}^{r=0.5t} rdf = 2\int_{r=0}^{r=0.5t} r\sigma dr = 2\int_{r=0}^{r=0.5t} rK\epsilon^n dr$$

$$= 2\int_{r=0}^{r=0.5t} rK\left(ln\left(1 + \frac{r}{R + 0.5t}\right)\right)^n dr$$

r : distance from the neutral axis

Appendix B: MATLAB Code Flow Chart

The MATLAB code divides the punch stroke to a number of increments (user selected) and for each increment the wrap angle is calculated from the punch position using Eq. 19. And the BHF_w is calculated as shown in the following chart:

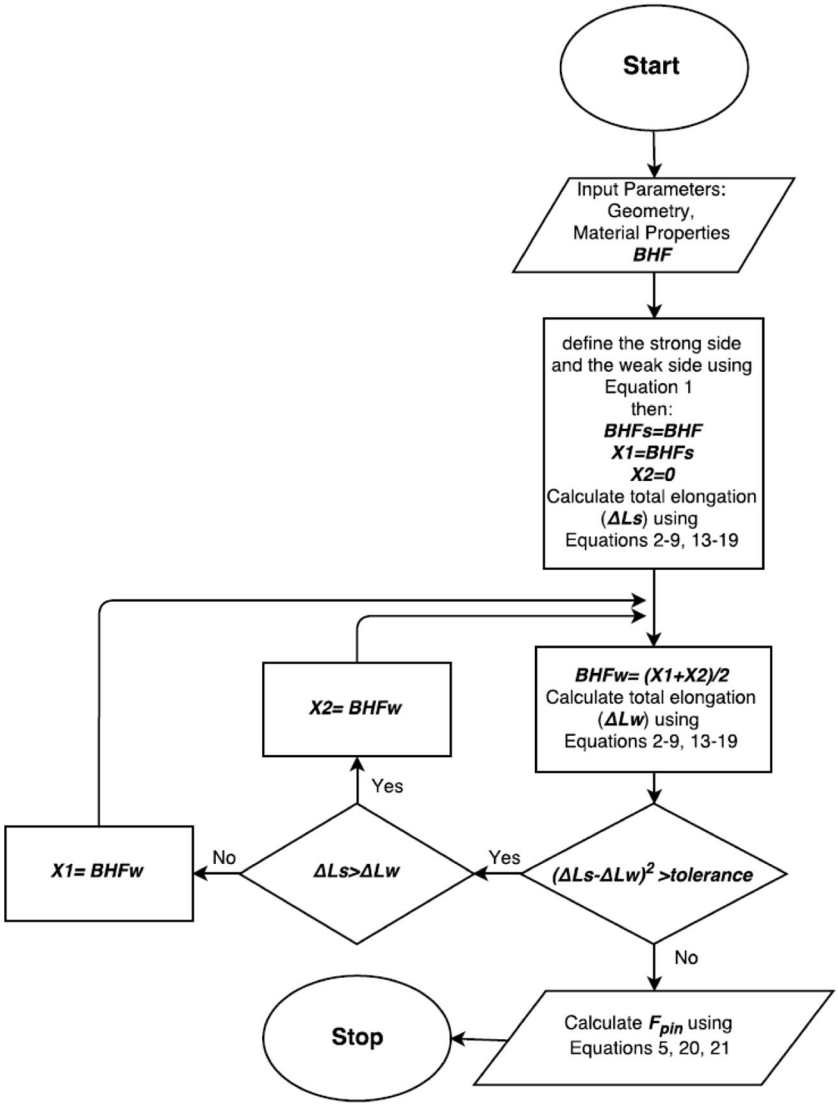

References

1. Saunders FI, Wagoner RH (1996) Forming of tailor-welded blanks. Metall Mater Trans A 27(9):2605–2616. https://doi.org/10.1007/BF02652354
2. Ahmetoglu MA, Brouwers D, Shulkin L, Taupin L, Kinzel GL, Altan T (1995) Deep drawing of round cups from tailor-welded blanks. J Mater Process Technol 53(3-4):684–694. https://doi.org/10.1016/0924-0136(94)01767-U
3. Kinsey BL, Cao J (1996) Enhancement of sheet metal formability via local adaptive controllers Brad L. Kinsey and Jian Cao Northwestern University. Mech Eng 1996
4. Morishita Y, Kado T, Abe S, Sakamoto Y, Yoshida F (2012) Role of counterpunch for square-cup drawing of tailored blank composed of thick/thin sheets. J Mater Process Technol 212(10):2102–2108. https://doi.org/10.1016/j.jmatprotec.2012.05.011
5. Heo Y, Choi Y, Kim HY, Seo D (2001) Characteristics of weld line movements for the deep drawing with drawbeads of tailor-welded

blanks. J Mater Process Technol 111(1-3):164–169. https://doi.org/10.1016/S0924-0136(01)00503-9

6. Chen W, Lin GS, Hu SJ (2008) A comparison study on the effectiveness of stepped binder and weld line clamping pins on formability improvement for tailor-welded blanks. J Mater Process Technol 207(1-3):204–210. https://doi.org/10.1016/j.jmatprotec.2007.12.100
7. He S, Wu X, Hu SJ (2003) Formability enhancement for tailor-welded blanks using blank holding force control. J Manuf Sci Eng 125(3):461–467. https://doi.org/10.1115/1.1580853
8. Kinsey BL, Cao J (2003) An analytical model for tailor welded blank forming. J Manuf Sci Eng 125(2):344. https://doi.org/10.1115/1.1537261
9. Kinsey B, Krishnan N, Cao J (2004) A methodology to reduce and quantify wrinkling in tailor welded blank forming. Int J Mater Prod Technol 21(1/2/3):154. https://doi.org/10.1504/IJMPT.2004.004749
10. Shazly M, Dawood B, Wifi AS, El-Mokadem A (2013). Effect of blank holder force schemes on weld-line movements in U-draw bending of tailor welded blanks. Paper presented at the Transactions of the North American Manufacturing Research Institution of SME. 41:105–113
11. Dawood Bishoy, Shazly Mostafa, Alaa Almokadem Abdalla S. Wifi (2015) Effect of variable blank holder force on the springback and weld-line movement during draw-bending of tailor welded blanks. In: 10th ASME 2015 Manuf. Sci. Eng. Conf. Pap. # MSEC2015–9379, June 8–12, 2015, Charlotte North Carolina, USA. pp 1–8
12. Marciniak Z, Duncan JL, Hu SJ (2002) Sheet deformation processes, In Mechanics of Sheet Metal Forming (Second Edition), Butterworth-Heinemann, Oxford. https://doi.org/10.1016/B978-075065300-8/50005-4
13. Taylor L, Cao J, Karafillis AP, Boyce MC (1995) Numerical simulations of sheet-metal forming. J Mater Process Technol 50(1-4):168–179. https://doi.org/10.1016/0924-0136(94)01378-E
14. Systèmes D Abaqus 6.14 example problems guide Volume I: Static and Dynamic Analyses
15. Zhao KM, Chun BK, Lee JK (2001) Finite element analysis of tailor-welded blanks. Finite Elem Anal Des 37(2):117–130. https://doi.org/10.1016/S0168-874X(00)00026-3